RELATIVISTIC COLLAPSE AND EXPLOSION OF ROTATING SUPERMASSIVE STARS WITH THERMONUCLEAR EFFECTS

Pedro J. Montero[1], Hans-Thomas Janka[1], and Ewald Müller[1]
(Dated: August 17, 2011)
Submitted for publication in the Astrophysical Journal

ABSTRACT

We present results of general relativistic simulations of collapsing supermassive stars with and without rotation using the two-dimensional general relativistic numerical code Nada, which solves the Einstein equations written in the BSSN formalism and the general relativistic hydrodynamics equations with high resolution shock capturing schemes. These numerical simulations use an equation of state which includes effects of gas pressure, and in a tabulated form those associated with radiation and the electron-positron pairs. We also take into account the effect of thermonuclear energy released by hydrogen and helium burning. We find that objects with a mass of $\approx 5 \times 10^5 \mathrm{M}_\odot$ and an initial metallicity greater than $Z_{CNO} \approx 0.007$ do explode if non-rotating, while the threshold metallicity for an explosion is reduced to $Z_{CNO} \approx 0.001$ for objects uniformly rotating. The critical initial metallicity for a thermonuclear explosion increases for stars with mass $\approx 10^6 \mathrm{M}_\odot$. For those stars that do not explode we follow the evolution beyond the phase of black hole formation. We compute the neutrino energy loss rates due to several processes that may be relevant during the gravitational collapse of these objects. The peak luminosities of neutrinos and antineutrinos of all flavors for models collapsing to a BH are $L_\nu \sim 10^{55}$erg/s. The total radiated energy in neutrinos varies between $E_\nu \sim 10^{56}$ ergs for models collapsing to a BH, and $E_\nu \sim 10^{45} - 10^{46}$ ergs for models exploding.

Subject headings: Supermassive stars

1. INTRODUCTION

There is large observational evidence of the presence of supermassive black holes (SMBHs) in the centres of most nearby galaxies (Rees 1998). The dynamical evidence related to the orbital motion of stars in the cluster surrounding Sgr A^* indicates the presence of a SMBH with mass $\approx 4 \times 10^6 \mathrm{M}_\odot$ (Genzel et al. 2000). In addition, the observed correlation between the central black hole masses and the stellar velocity dispersion of the bulge of the host galaxies suggests a direct connection between the formation and evolution of galaxies and SMBHs (Kormendy & Gebhardt 2001).

The observation of luminous quasars detected at redshifts higher than 6 in the Sloan Digital Sky Survey (SDSS) implies that SMBHs with masses $\sim 10^9 \mathrm{M}_\odot$, which are believed to be the engines of such powerful quasars, were formed within the first billion years after the Big Bang (e.g. Fan 2006 for a recent review). However, it is still an open question how SMBH seeds form and grow to reach such high masses in such a short amount of time (Rees 2001).

A number of different routes based on stellar dynamical processes, hydrodynamical processes or a combination of both have been suggested (e.g. Volonteri 2010 for a recent review). One of the theoretical scenarios for SMBH seed formation is the gravitational collapse of the first generation of stars (Population III stars) with masses $M \sim 100 \mathrm{M}_\odot$ that are expected to form in halos with virial temperature $T_{vir} < 10^4 K$ at $z \sim 20 - 50$ where cooling by molecular hydrogen is effective. As a result of the gravitational collapse of such Pop III stars, very

massive BHs would form and then grow via merger and accretion (Haiman & Loeb 2001; Yoo & Miralda-Escudé 2004; Alvarez et al. 2009).

Another possible scenario proposes that if sufficient primordial gas in massive halos, with mass $\sim 10^8 M_\odot$, is unable to cool below $T_{vir} \gtrsim 10^4 K$, it may lead to the formation of a supermassive object (Bromm & Loeb 2003; Begelman et al. 2006), which would eventually collapse to form a SMBH. This route assumes that fragmentation, which depends on efficient cooling, is suppressed, possibly by the presence of sufficiently strong UV radiation, that prevents the formation of molecular hydrogen in an environment with metallicity smaller than a given critical value (Santoro & Shull 2006; Omukai et al. 2008). Furthermore, fragmentation may depend on the turbulence present within the inflow of gas, and on the mechanism redistributing its angular momentum (Begelman & Shlosman 2009). The "bars-within-bars" mechanism (Shlosman et al. 1989; Begelman et al. 2006) is a self-regulating route to redistribute angular momentum and sustain turbulence such that the inflow of gas can proceed without fragmenting as it collapses even in a metal-enriched environment.

Depending on the rate and efficiency of the inflowing mass, there may be different outcomes. A low rate of mass accumulation would favor the formation of isentropic supermassive stars (SMSs), with mass $\geq 5 \times 10^4 M_\odot$, which then would evolve as equilibrium configurations dominated by radiation pressure (Iben 1963; Hoyle & Fowler 1963; Fowler 1964). A different outcome could result if the accumulation of gas is fast enough so that the outer layers of SMSs are not thermally relaxed during much of their lifetime, thus having an entropy stratification (Begelman 2009).

A more exotic mechanism that could eventually lead to

montero@mpa-garching.mpg.de
[1] Max-Planck-Institut für Astrophysik, Karl-Schwarzschild-Str. 1, D-85748 Garching, Germany;

a SMS collapsing into a SMBH is the formation and evolution of supermassive dark matter stars (SDMS) (Spolyar et al 2008). Such stars would be composed primarily of hydrogen and helium with only about 0.1% of their mass in the form of dark matter, however they would shine due to dark matter annihilation. It has recently been pointed out that SDMSs could reach masses $\sim 10^5 M_\odot$ (Freese et al. 2010). Once SDMSs run out of their dark matter supply, they experience a contraction phase that increases their baryon density and temperature, leading to an environment where nuclear burning may become important for the subsequent stellar evolution.

If isentropic SMSs form, their quasi-stationary evolution of cooling and contraction will drive the stars to the onset of a general relativistic gravitational instability leading to their gravitational collapse (Chandrasekhar 1964; Fowler 1964), and possibly also to the formation of a SMBH. The first numerical simulations, within the post-Newtonian approximation, of Appenzeller & Fricke (1972) concluded that for spherical stars with masses greater than $10^6 M_\odot$ thermonuclear reactions have no major effect on the collapse, while less massive stars exploded due to hydrogen burning. Later Shapiro & Teukolsky (1979) performed the first relativistic simulations of the collapse of a SMS in spherical symmetry. They were able to follow the evolution until the formation of a BH, although their investigations did not include any microphysics. Fuller et al. (1986) revisited the work of Appenzeller & Fricke (1972) and performed simulations of non-rotating SMSs in the range of 10^5-$10^6 M_\odot$ with post-Newtonian corrections and detailed microphysics that took into account an equation of state (EOS) including electron-positron pairs, and a reaction network describing hydrogen burning by the CNO cycle and its break-out via the rapid proton capture (rp)-process. They found that SMSs with zero initial metallicity do not explode, while SMSs with masses larger than $10^5 M_\odot$ and with metallicity $Z_{CNO} \geq 0.005$ do explode.

More recently Linke et al. (2001) carried out general relativistic hydrodynamic simulations of the spherically symmetric gravitational collapse of SMSs adopting a spacetime foliation with outgoing null hypersurfaces to solve the system of Einstein and fluid equations. They performed simulations of spherical SMSs with masses in the range of $5 \times 10^5 M_\odot - 10^9 M_\odot$ using an EOS that accounts for contributions from baryonic gases, and in a tabulated form, radiation and electron-positron pairs. They were able to follow the collapse from the onset of the instability until the point of BH formation, and showed that an apparent horizon enclosing about 25% of the stellar material was formed in all cases when simulations stopped.

Shibata & Shapiro (2002) carried out general relativistic numerical simulations in axisymmetry of the collapse of uniformly rotating SMSs to BHs. They did not take into account thermonuclear burning, and adopted a Γ-law EOS, $P = (\Gamma - 1)\rho\epsilon$ with adiabatic index $\Gamma = 4/3$, where P is the pressure, ρ the rest-mass density, and ϵ the specific internal energy. Although their simulations stopped before the final equilibrium was reached, the BH growth was followed until about 60% of the mass had been swallowed by the SMBH. They estimated that

about 90% of the total mass would end up in the final SMBH with a spin parameter of $J/M^2 \sim 0.75$.

The gravitational collapse of differentially rotating SMSs in three dimensions was investigated by Saijo & Hawke (2009), who focused on the post-BH evolution, and also on the gravitational wave (GW) signal resulting from the newly formed SMBH and the surrounding disk. The GW signal is expected to be emitted in the low frequency LISA band ($10^{-4} - 10^{-1}$ Hz).

Despite the progress made, the final fate rotating isentropic SMSs is still unclear. In particular, it is still an open question for which initial metallicities hydrogen burning by the β-limited hot CNO cycle and its break-out via the $^{15}O(\alpha, \gamma)^{19}Ne$ reaction (rp-process) can halt the gravitational collapse of rotating SMSs and generate enough thermal energy to lead to an explosion. To address this issue, we perform a series of general relativistic hydrodynamic simulations with a microphysical EOS accounting for contributions from radiation, electron-positron pairs, and baryonic matter, and taking into account the net thermonuclear energy released by the nuclear reactions involved in hydrogen burning through the pp-chain, cold and hot CNO cycles and their break-out by the rp-process, and helium burning through the 3-α reaction. The numerical simulations were carried out with the Nada code (Montero et al. 2008), which solves the Einstein equations coupled to the general relativistic hydrodynamics equations.

Greek indices run from 0 to 3, Latin indices from 1 to 3, and we adopt the standard convention for the summation over repeated indices. Unless otherwise stated we use units in which $c = G = 1$.

2. BASIC EQUATIONS

Next we briefly describe how the system of Einstein and hydrodynamic equations are implemented in the Nada code. We refer to Montero et al. (2008) for a more detailed description of the main equations and thorough testing of the code (namely single BH evolutions, shock tubes, evolutions of both spherical and rotating relativistic stars, gravitational collapse to a BH of a marginally stable spherical star, and simulations of a system formed by a BH surrounded by a self-gravitating torus in equilibrium).

2.1. *Formulation of Einstein equations*
2.1.1. *BSSN formulation*

We follow the 3+1 formulation in which the spacetime is foliated into a set of non-intersecting spacelike hypersurfaces. In this approach, the line element is written in the following form

$$ds^2 = -(\alpha^2 - \beta_i\beta^i)dt^2 + 2\beta_i dx^i dt + \gamma_{ij}dx^i dx^j, \quad (1)$$

where α, β^i and γ_{ij} are the lapse function, the shift three-vector, and the three-metric, respectively. The latter is defined by

$$\gamma_{\mu\nu} = g_{\mu\nu} + n_\mu n_\nu, \quad (2)$$

where n^μ is a timelike unit-normal vector orthogonal to a spacelike hypersurface.

We make use of the BSSN formulation (Nakamura 1987; Shibata & Nakamura 1995; Baumgarte & Shapiro

1999) to solve the Einstein equations. Initially, a conformal factor ϕ is introduced, and the conformally related metric is written as

$$\tilde{\gamma}_{ij} = e^{-4\phi}\gamma_{ij} \qquad (3)$$

such that the determinant of the conformal metric, $\tilde{\gamma}_{ij}$, is unity and $\phi = \ln(\gamma)/12$, where $\gamma = \det(\gamma_{ij})$. We also define the conformally related traceless part of the extrinsic curvature K_{ij},

$$\tilde{A}_{ij} = e^{-4\phi}A_{ij} = e^{-4\phi}\left(K_{ij} - \frac{1}{3}\gamma_{ij}K\right), \qquad (4)$$

where K is the trace of the extrinsic curvature. We evolve the conformal factor defined as $\chi \equiv e^{-4\phi}$ (Campanelli et al. 2006), and the auxiliary variables $\tilde{\Gamma}^i$, known as the *conformal connection functions*, defined as

$$\tilde{\Gamma}^i \equiv \tilde{\gamma}^{jk}\tilde{\Gamma}^i{}_{jk} = -\partial_j\tilde{\gamma}^{ij}, \qquad (5)$$

where $\tilde{\Gamma}^i{}_{jk}$ are the connection coefficients associated with $\tilde{\gamma}_{ij}$.

During the evolution we also enforce the constraints $\mathrm{Tr}(\tilde{A}_{ij}) = 0$ and $\det(\tilde{\gamma}_{ij}) = 1$ at every time step.

We use the Cartoon method (Alcubierre et al. 2001) to impose axisymmetry while using Cartesian coordinates.

2.1.2. *Gauge choices*

In addition to the BSSN spacetime variables $(\tilde{\gamma}_{ij}, \tilde{A}_{ij}, K, \chi, \tilde{\Gamma}^i)$, there are two more quantities left undetermined, the lapse, α and the shift vector β^i. We used the so-called "non-advective 1+log" slicing (Bona et al. 1997), by dropping the advective term in the "1+log" slicing condition. In this case, the slicing condition takes the form

$$\partial_t\alpha = -2\alpha K. \qquad (6)$$

For the shift vector, we choose the "Gamma-freezing condition" (Alcubierre et al. 2003) written as

$$\partial_t\beta^i = \frac{3}{4}B^i, \qquad (7)$$

$$\partial_t B^i = \partial_t\tilde{\Gamma}^i - \eta B^i, \qquad (8)$$

where η is a constant that acts as a damping term, originally introduced both to prevent long term drift of the metric functions and to prevent oscillations of the shift vector.

2.2. *Formulation of the hydrodynamics equations*

The general relativistic hydrodynamics equations, expressed through the conservation equations for the stress-energy tensor $T^{\mu\nu}$ and the continuity equation are

$$\nabla_\mu T^{\mu\nu} = 0 \, , \qquad \nabla_\mu(\rho u^\mu) = 0, \qquad (9)$$

where ρ is the rest-mass density, u^μ is the fluid four-velocity and ∇ is the covariant derivative with respect to the spacetime metric. Following Shibata (2003), the general relativistic hydrodynamics equations are written in a conservative form in cylindrical coordinates. Since the Einstein equations are solved only in the $y = 0$ plane with Cartesian coordinates (2D), the hydrodynamic equations are rewritten in Cartesian coordinates for $y = 0$. The following definitions for the hydrodynamical variables are used

$$\rho_* \equiv \rho W e^{6\phi}, \qquad (10)$$

$$v^i \equiv \frac{u^i}{u^t} = -\beta^i + \alpha\gamma^{ij}\frac{\hat{u}_j}{hW}, \qquad (11)$$

$$\hat{u}_i \equiv hu_i, \qquad (12)$$

$$\hat{e} \equiv \frac{e^{6\phi}}{\rho_*}T_{\mu\nu}n^\mu n^\nu = hW - \frac{P}{\rho W}, \qquad (13)$$

$$W \equiv \alpha u^t, \qquad (14)$$

where W and h are the Lorentz factor and the specific fluid enthalpy respectively, and P is the pressure. The conserved variables are ρ_*, $J_i = \rho_*\hat{u}_i$, $E_* = \rho_*\hat{e}$. We refer to Shibata (2003) for further details.

3. SUPERMASSIVE STARS AND MICROPHYSICS
3.1. *Properties of SMSs*

Isentropic SMSs are self-gravitating equilibrium configurations of masses in the range of $10^4 - 10^8\mathrm{M}_\odot$, which are mainly supported by radiation pressure, while the pressure of electron-positron pairs and of the baryon gas are only minor contributions to the EOS. Such configurations are well described by Newtonian polytropes with polytropic index $n = 3$ (adiabatic index $\Gamma = 4/3$). The ratio of gas pressure to the total pressure (β) for spherical SMSs can be written as (Fowler & Hoyle 1966)

$$\beta = \frac{P_g}{P_{tot}} \approx \frac{4.3}{\mu}\left(\frac{M_\odot}{M}\right)^{1/2}, \qquad (15)$$

where μ is the mean molecular weight. Thus $\beta \approx 10^{-2}$ for $M \approx 10^6\mathrm{M}_\odot$.

Since nuclear burning timescales are too long for $M \gtrsim 10^4\mathrm{M}_\odot$, evolution of SMSs proceeds on the Kelvin-Helmholtz timescale and is driven by the loss of energy and entropy by radiation as well as loss of angular momentum via mass shedding in the case of rotating configurations.

Although corrections due to the nonrelativistic gas of baryons and electrons and general relativistic effects are small, they cannot be neglected for the evolution. Firstly, gas corrections raise the adiabatic index slightly above $4/3$

$$\Gamma \approx \frac{4}{3} + \frac{\beta}{6} + 0(\beta^2). \qquad (16)$$

Secondly, general relativistic corrections lead to the existence of a maximum for the equilibrium mass as a function of the central density. For spherical SMSs this means that for a given mass the star evolves to a critical density beyond which it is dynamically unstable against radial perturbations (Chandrasekhar 1964):

$$\rho_{crit} = 1.994 \times 10^{18}\left(\frac{0.5}{\mu}\right)^3\left(\frac{M_\odot}{M}\right)^{7/2} \mathrm{gcm}^{-3}. \qquad (17)$$

The onset of the instability also corresponds to a critical value of the adiabatic index Γ_{crit}, i.e. configurations

become unstable when the adiabatic index drops below the critical value

$$\Gamma_{crit} = \frac{4}{3} + 1.12 \frac{2GM}{Rc^2}. \qquad (18)$$

This happens when the stabilizing gas contribution to the EOS does not raise the adiabatic index above $4/3$ to compensate for the destabilizing effect of general relativity expressed by the second term on the righ-hand-side of Eq. (18).

Rotation can stabilize configurations against the radial instability. The stability of rotating SMSs with uniform rotation was analyzed by Baumgarte & Shapiro (1999a,b). They found that stars at the onset of the instability have an equatorial radius $R \approx 640GM/c^2$, a spin parameter $q \equiv cJ/GM^2 \approx 0.97$, and a ratio of rotational kinetic energy to the gravitational binding energy of $T/W \approx 0.009$.

3.2. Equation of State

To close the system of hydrodynamic equations (Eq. 9) we need to define the EOS. We follow a treatment which includes separately the baryon contribution on the one hand, and photons and electron-positron pairs contributions, in a tabulated form, on the other hand. The baryon contribution is given by the analytic expressions for the pressure and specific internal energy

$$P_b = \frac{\mathcal{R}\rho T}{\mu_b}, \qquad (19)$$

$$\epsilon_b = \frac{2}{3} \frac{\mathcal{R}\rho T}{\mu_b}, \qquad (20)$$

where $\mathcal{R}$ the universal gas constant, T the temperature, ϵ_b the baryon specific internal energy, and μ_b is the mean molecular weight due to ions, which can be expressed as a function of the mass fractions of hydrogen (X), helium (Y) and heavier elements (metals) (Z_{CNO}) as

$$\frac{1}{\mu_b} \approx X + \frac{Y}{4} + \frac{Z_{CNO}}{\langle A \rangle}, \qquad (21)$$

where $\langle A \rangle$ is the average atomic mass of the heavy elements. We assume that the composition of SMSs (approximately that of primordial gas) has a mass fraction of hydrogen $X = 0.75 - Z_{CNO}$ and helium $Y = 0.25$, where the metallity $Z_{CNO} = 1 - X - Y$ is an initial parameter, typically of the order of $Z_{CNO} \sim 10^{-3}$ (see Table 1 details). Thus, for the initial compositions that we consider the mean molecular weight of baryons is $\mu_b \approx 1.23$ (i.e. corresponding to a molecular weight for both ions and electrons of $\mu \approx 0.59$).

Effects associated with photons and the creation of electron-positron pairs are taken into account employing a tabulated EOS. At temperatures above 10^9K, not all the energy is used to increase the temperature and pressure, but part of the photon energy is used to create the rest-mass of the electron-positron pairs. As a result of pair creation, the adiabatic index of the star decreases, which means that the stability of the star is reduced.

Given the specific internal energy, ϵ and rest-mass density, ρ, as evolved by the hydrodynamic equations, it is possible to compute the temperature T by a Newton-Raphson algorithm that solves the equation $\epsilon^*(\rho, T) = \epsilon$ for T,

$$T_{n+1} = T_n - (\epsilon^*(\rho, T_n) - \epsilon) \left(\frac{\partial \epsilon^*(\rho, T)}{\partial T}\right)^{-1}\Bigg|_{T_n}, \qquad (22)$$

where n is the iteration counter.

3.3. Nuclear burning

In order to avoid the small time steps, and CPU-time demands connected with the solution of a nuclear reaction network coupled to the hydrodynamic evolution, we apply an approximate method to take into account the basic effects of nuclear burning on the dynamics of the collapsing SMSs. We compute the nuclear energy release rates by hydrogen burning (through the pp-chain, cold and hot CNO cycles, and their break-out by the rp-process) and helium burning (through the 3-α reaction) as a function of rest-mass density, temperature and mass fractions of hydrogen X, helium Y and CNO metallicity Z_{CNO}. These nuclear energy generation rates are added as a source term on the right-hand-side of the evolution equation for the conserved quantity E_*.

The change rates of the energy density due to nuclear reactions, in the fluid frame, expressed in units of [erg cm^{-3} s^{-1}] are given by:

- pp-chain (Clayton 1983):

$$\left(\frac{\partial e}{\partial t}\right)_{pp} = \rho(2.38 \times 10^6 \rho g_{11} X^2 T_6^{-0.6666}$$
$$e^{-33.80/T_6^{0.3333}}), \qquad (23)$$

  where $T_6 = T/10^6$K, and g_{11} is given by

$$g_{11} = 1 + 0.0123 T_6^{0.3333} + 0.0109 T_6^{0.66666} +$$
$$0.0009 T_6. \qquad (24)$$

- 3-α (Wiescher et al. 1999):

$$\left(\frac{\partial e}{\partial t}\right)_{3\alpha} = \rho(5.1 \times 10^8 \rho^2 Y^3 T_9^{-3} e^{-4.4/T_9}), \qquad (25)$$

  where $T_9 = T/10^9$K.

- Cold-CNO cycle (Shen & Bildsten 2007):

$$\left(\frac{\partial e}{\partial t}\right)_{CCNO} = 4.4 \times 10^{25} \rho^2 X Z_{CNO}$$
$$(T_9^{-2/3} e^{-15.231/T_9^{1/3}} +$$
$$+ 8.3 \times 10^{-5} T_9^{-3/2} e^{-3.0057/T_9}). \qquad (26)$$

- Hot-CNO cycle (Wiescher et al. 1999):

$$\left(\frac{\partial e}{\partial t}\right)_{HCNO} = 4.6 \times 10^{15} \rho Z_{CNO}. \qquad (27)$$

- rp-process (Wiescher et al. 1999):

$$\left(\frac{\partial e}{\partial t}\right)_{rp} = \rho(1.77 \times 10^{16}\rho Y Z_{CNO}$$

$$29.96 T_9^{-3/2} e^{-5.85/T_9}). \tag{28}$$

Since we follow a single fluid approach, in which we solve only the hydrodynamics equations Eq. (9) (i.e. we do not solve additional advection equations for the abundances of hydrogen, helium and metals), the elemental abundances during the time evolution are fixed. Nevertheless, this assumption most possibly does not affect significantly the estimate of the threshold metallicity needed to produce a thermal bounce in collapsing SMSs. The average energy release through the 3-α reaction is about 7.275 MeV for each ^{12}C nucleus formed. Since the total energy due to helium burning for exploding models is $\sim 10^{45}$ ergs (e.g. 9.0×10^{44} ergs for model S1.c); and even considering that this energy is released mostly in a central region of the SMS containing $10^4 M_\odot$ of its rest-mass (Fuller et al. 1986), it is easy to show that the change in the metallicity is of the order of 10^{-11}. Therefore, the increase of the metallicity in models experiencing a thermal bounce is much smaller than the critical metallicities needed to trigger the explosions. Similarly, the average change in the mass fraction of hydrogen due to the cold and hot CNO cycles is expected to be $\sim 10\%$ for exploding models.

3.4. *Recovery of the primitive variables*

After each time iteration the conserved variables (i.e. $\rho_*, J_x, J_y, J_z, E_*$) are updated and the *primitive* hydrodynamical variables (i.e. $\rho, v^x, v^y, v^z, \epsilon$) have to be recovered. The recovery is done in such a way that it allows for the use of a general EOS of the form $P = P(\rho, \epsilon)$. We calculate a function $f(P^*) = P(\rho^*, \epsilon^*) - P^*$, where ρ^* and ϵ^* depend only on the conserved quantities and the pressure guess P^*. The new pressure is computed then iteratively by a Newton-Raphson method until the desired convergence is achieved.

3.5. *Energy loss by neutrino emission*

The EOS allows us to compute the neutrino losses due to the following processes, which become most relevant just before BH formation:

- Pair annihilation ($e^+ + e^- \rightarrow \bar{\nu} + \nu$): most important process above 10^9K. Due to the large mean free path of neutrinos in the stellar medium at the densities of SMSs the energy loss by neutrinos can be significant. For a $10^6 M_\odot$ SMS most of the energy release in the form of neutrinos originates from this process. The rates are computed using the fitting formula given by Itoh et al. (1996).

- Photo-neutrino emission ($\gamma + e^\pm \rightarrow e^\pm + \bar{\nu} + \nu$): dominates at low temperatures $T \lesssim 4 \times 10^8$K and densities $\rho \lesssim 10^5$gcm^{-3} (Itoh et al. 1996).

- Plasmon decay ($\gamma \rightarrow \bar{\nu} + \nu$): This is the least relevant process for the conditions encountered by the models we have considered because its importance increases at higher densities than those present in

SMSs. The rates are computed using the fitting formula given by Haft et al. (1994).

4. COMPUTATIONAL SETUP

The evolution equations are integrated by the method of lines, for which we use an optimal strongly stability-preserving (SSP) Runge-Kutta algorithm of fourth-order with 5 stages (Spiteri & Ruuth 2002). We use a second-order slope limiter reconstruction scheme (MC limiter) to obtain the left and right states of the primitive variables at each cell interface, and a HLLE approximate Riemann solver (Harten et al. 1983; Einfeldt 1988) to compute the numerical fluxes in the x and z directions.

Derivative terms in the spacetime evolution equations are represented by a fourth-order centered finite-difference approximation on a uniform Cartesian grid except for the advection terms (terms formally like $\beta^i \partial_i u$), for which an upwind scheme is used.

The computational domain is defined as $0 \leq x \leq L$ and $0 \leq z \leq L$, where L refers to the location of the outer boundaries. We used a cell-centered Cartesian grid to avoid that the location of the BH singularity coincides with a grid point.

4.1. *Regridding*

Since it is not possible to follow the gravitational collapse of a SMS from the early stages to the phase of black hole formation with a uniform Cartesian grid (the necessary fine zoning would be computationally too demanding), we adopt a regridding procedure (Shibata & Shapiro 2002). During the initial phase of the collapse we rezone the computational domain by moving the outer boundary inward, decreasing the grid spacing while keeping the initial number of grid points fixed. Initially we use $N \times N = 400 \times 400$ grid points, and place the outer boundary at $L \approx 1.5 r_e$ where r_e is the equatorial radius of the star. Rezoning onto the new grid is done using a polynomial interpolation. We repeat this procedure 3-4 times until the collapse timescale in the central region is much shorter than in the outer parts. At this point, we both decrease the grid spacing and also increase the number of grid points N in dependence of the lapse function typically as follows: $N \times N = 800 \times 800$ if $0.8 > \alpha > 0.6$, $N \times N = 1200 \times 1200$ if $0.6 > \alpha > 0.4$, and $N \times N = 1800 \times 1800$ if $\alpha < 0.4$. This procedure ensures the error in the conservation of the total rest-mass to be less than 2% on the finest computational domain.

4.2. *Hydro-Excision*

To deal with the spacetime singularity from the newly formed BH we use the method of excising the matter content in a region within the horizon as proposed by Hawke et al. (2005) once an apparent horizon (AH) is found. This excision is done only for the hydrodynamical variables, and the coordinate radius of the excised region is allowed to increase in time. On the other hand, we do neither use excision nor artificial dissipation terms for the spacetime evolution, and solely rely on the gauge conditions.

4.3. *Definitions*

Here we define some of the quantities listed in Table 1. We compute the total rest-mass M_* and the ADM mass

TABLE 1
MAIN PROPERTIES OF THE INITIAL MODELS STUDIED. FROM LEFT TO RIGHT THE COLUMNS SHOW: MODEL, GRAVITATIONAL MASS, INITIAL
CENTRAL REST-MASS DENSITY, $T_k/|W|$, ANGULAR VELOCITY, INITIAL CENTRAL TEMPERATURE, METALLICITY, THE FATE OF THE STAR, RADIAL
KINETIC ENERGY AFTER THERMAL BOUNCE, AND TOTAL NEUTRINO ENERGY OUTPUT.

Model	M $[10^5 \mathrm{M}_\odot]$	ρ_c $[10^{-2}\mathrm{g/cm^3}]$	$T_k/|W|$	Ω $[10^{-5}\mathrm{rad/s}]$	T_c $[10^7\mathrm{K}]$	Initial metallicity $[10^{-3}]$	Fate	E_{RK} $[10^{56}\mathrm{erg}]$	E_ν $[\mathrm{erg}]$
S1.a	5	2.4	0	0	5.8	5	BH	...	3.4×10^{56}
S1.b	5	2.4	0	0	5.8	6	BH	..	...
S1.c	5	2.4	0	0	5.8	7	Explosion	5.5	9.4×10^{45}
R1.a	5	40	0.0088	2.49	13	0.5	BH	...	5.4×10^{56}
R1.b	5	40	0.0088	2.49	13	0.8	BH	...	...
R1.c	5	40	0.0088	2.49	13	1	Explosion	1.0	...
R1.d	5	40	0.0088	2.49	13	2	Explosion	1.9	8.9×10^{45}
S2.a	10	0.23	0	0	2.6	30	BH	...	6.8×10^{56}
S2.b	10	0.23	0	0	2.6	50	Explosion	35	8.0×10^{46}
R2.a	10	12	0.0087	1.47	9.7	0.5	BH	...	3.1×10^{56}
R2.b	10	12	0.0087	1.47	9.7	0.8	BH	...	...
R2.c	10	12	0.0087	1.47	9.7	1.0	BH	...	...
R2.d	10	12	0.0087	1.47	9.7	1.5	Explosion	1.5	2.1×10^{46}

M as

$$M_* = 4\pi \int_0^L x dx \int_0^L \rho_* dz, \qquad (29)$$

$$M = -2 \int_0^L x dx \int_0^L dz \left[-2\pi E e^{5\phi} + \frac{e^\phi}{8}\tilde{R} \right.$$
$$\left. -\frac{e^{5\phi}}{8}\left(\tilde{A}_{ij}\tilde{A}^{ij} - \frac{2}{3}K^2 \right) \right], \quad (30)$$

where $E = n_\mu n_\nu T^{\mu\nu}$ (n^μ being the unit normal to the hypersurface) and $\tilde{R}$ is the scalar curvature associated to the conformal metric $\tilde{\gamma}_{ij}$.

The rotational kinetic energy T_k and the gravitational potential energy W are given by

$$T_k = 2\pi \int_0^L x^2 dx \int_0^L \rho_* \hat{u}_y \Omega dz, \qquad (31)$$

where Ω is the angular velocity.

$$W = M - (M_* + T_k + E_{int}), \qquad (32)$$

where the internal energy is computed as

$$E_{int} = 4\pi \int_0^L x dx \int_0^L \rho_* \epsilon dz. \qquad (33)$$

In axisymmetry the AH equation becomes a nonlinear ordinary differential equation for the AH shape function, $h = h(\theta)$ (Shibata 1997; Thornburg 2007). We employ an AH finder that solves this ODE by a shooting method using $\partial_\theta h(\theta = 0) = 0$ and $\partial_\theta h(\theta = \pi/2) = 0$ as boundary conditions. We define the mass of the AH as

$$M_{\mathrm{AH}} = \sqrt{\frac{\mathcal{A}}{16\pi}}, \qquad (34)$$

where $\mathcal{A}$ is the area of the AH.

5. INITIAL MODELS

The initial SMSs are set up as isentropic objects. All models are chosen such that they are gravitationally unstable, and therefore their central rest-mass density is slightly larger than the critical central density required

for the onset of the collapse of a configuration with given mass and entropy. A list of the different SMSs we have considered is provided in Table 1. Models S1 and S2 represent a spherically symmetric, nonrotating SMS with gravitational mass of $M = 5 \times 10^5 \mathrm{M}_\odot$ and $M = 1 \times 10^6 \mathrm{M}_\odot$, respectively, while models R1 and R2 are uniformly rotating initial models again with masses of $M = 5 \times 10^5 \mathrm{M}_\odot$ and $M = 1 \times 10^6 \mathrm{M}_\odot$, respectively. The rigidly and maximally rotating initial models R1 and R2 are computed with the Lorene code (URL http://www.lorene.obspm.fr). We also introduce a perturbation to trigger the gravitational collapse by reducing the pressure overall by $\approx 1.5\%$.

In order to determine the threshold metallicity required to halt the collapse and produce an explosion we carry out several numerical simulations for each initial model with different values of the initial metallicity. The initial metallicities along with the fate of the star are given in Table 1.

6. RESULTS

6.1. Collapse to BH vs. Thermonuclear explosion

First we consider a gravitationally unstable spherically symmetric SMS with a gravitational mass of $M = 5 \times 10^5 \mathrm{M}_\odot$ (S1.a, S1.b and S1.c), which corresponds to a model extensively discussed in Fuller et al. (1986), and therefore allows for a comparison with the results presented here. Fuller et al. (1986) found that unstable spherical SMSs with $M = 5 \times 10^5 \mathrm{M}_\odot$ and an initial metallicity $Z_{CNO} = 2 \times 10^{-3}$ collapse to a BH while models with an initial metallicity $Z_{CNO} = 5 \times 10^{-3}$ explode due to the nuclear energy released by the hot CNO burning. They also found that the central density and temperature at thermal bounce (where the collapse is reversed to an explosion) are $\rho_{c,b} = 3.16$ g/cm^3 and $T_{c,b} = 2.6 \times 10^8$ K, respectively.

The left panels in Figure 1 show the time evolution of the central rest-mass density (upper panel) and central temperature (lower panel) for models S1.a, S1.c, R1.a and R1.d, i.e., non-rotating and rotating models with a mass of $M = 5 \times 10^5 \mathrm{M}_\odot$. In particular, the solid lines represent the time evolution of the central density and temperature for model S1.c ($Z_{CNO} = 7 \times 10^{-3}$) and R1.d
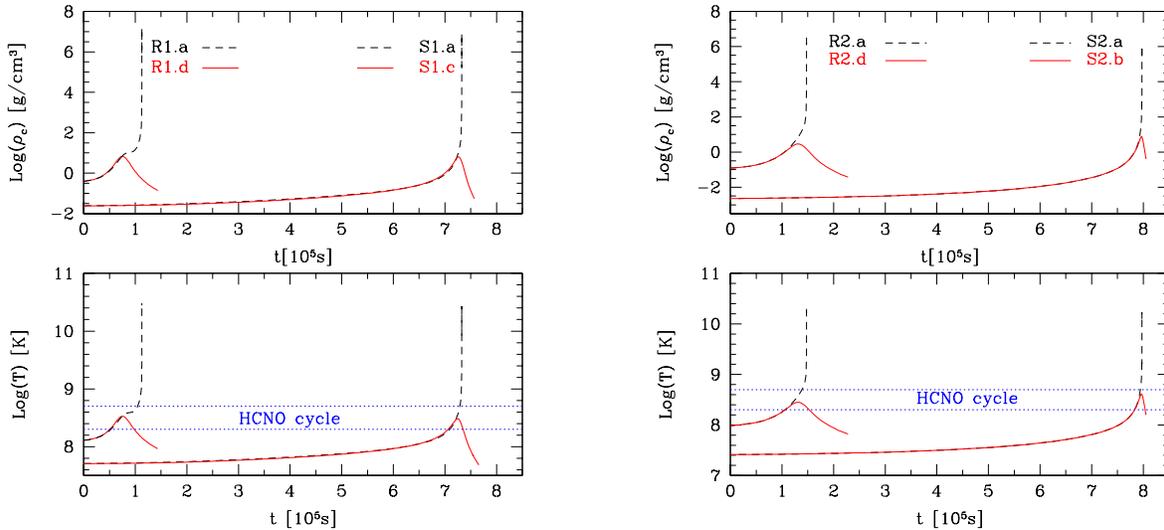
FIG. 1.— Left upper panel shows the time evolution of the central rest-mass density for models S1 and R1 (i.e., spherical and rotating stars with mass $M = 5 \times 10^5 \mathrm{M}_\odot$), and the lower left panel shows the time evolution of the central temperature. Horizontal dotted lines mark the temperature range in which nuclear energy is primarily released by the hot CNO cycle. Similarly, the time evolution of the same quantities for model S2 and R2 (i.e., spherical and rotating stars with mass $M = 1 \times 10^6 \mathrm{M}_\odot$) are shown in the upper and lower right panels. As the collapse proceeds, the central density and temperature rise rapidly, increasing the nuclear energy generation rate by hydrogen burning. If the metallicity is sufficiently high, enough energy can be liberated to produce a thermal bounce. This is the case for models S1.c, R1.d, S2.b and R2.d shown here.

$(Z_{CNO} = 5 \times 10^{-4})$. As the collapse proceeds, the central density and temperature rise rapidly, which increases the nuclear energy generation rate by hydrogen burning. Since the metallicity is sufficiently high, enough energy can be liberated to increase the pressure and to produce a thermal bounce. This is the case for model S1.c. In Figure 1 we show that a thermal bounce occurs (at approximately $t \sim 7 \times 10^5$ s) entirely due to the hot CNO cycle, which is the main source of thermonuclear energy at temperatures in the range $2 \times 10^8 \mathrm{K} \leq \mathrm{T} \leq 5 \times 10^8 \mathrm{K}$. The rest-mass density at bounce is $\rho_{c,b} = 4.8$ g/cm^3 and the temperature $T_{c,b} = 3.05 \times 10^8$K. These values, as well as the threshold metallicity needed to trigger a thermonuclear explosion $(Z_{CNO} = 7 \times 10^{-3})$, are higher than those found by Fuller et al. (1986) (who found that a spherical nonrotating model with the same rest-mass would explode, if the initial metallicity was $Z_{CNO} = 5 \times 10^{-3}$).

On the other hand, dashed lines show the time evolution of the central density and temperature for model S1.a $(Z_{CNO} = 5 \times 10^{-3})$. In this case, as well as for model S1.b, the collapse is not halted by the energy release and continues until an apparent horizon is found, indicating the formation of a BH.

We note that the radial velocity profiles change continuously near the time where the collapse is reversed to an explosion due to the nuclear energy released by the hot CNO burning, and an expanding shock forms only near the surface of the star at a radius $R \approx 1.365 \times 10^{13}$cm (i.e. $R/M \approx 180$) where the rest-mass density is $\approx 3.5 \times 10^{-6}$gcm^{-3}. We show in Figure 2 the profiles of the x-component of the three-velocity v^x along the x-axis (in the equatorial plane) for the nonrotating spherical stars S1.a (dashed lines) and S1.c (solid lines) at three different time slices near the time at which model S1.c experiences a thermal bounce. Velocity profiles of model S1.c are displayed up to the radius where a shock forms

at $t \approx 7.31 \times 10^5$s and begins to expand into the low density outer layers of the SMS.

The evolutionary tracks for the central density and temperature of the rotating models R1.a and R1.d are also shown in Figure 1. A dashed line corresponds to model R1.a, with an initial metallicity $Z_{CNO} = 5 \times 10^{-4}$, which collapses to a BH. A solid line denotes model R1.d with $Z_{CNO} = 2 \times 10^{-3}$, which explodes due to the energy released by the hot CNO cycle. We find that Model R1.c with a lower metallicity of $Z_{CNO} = 1 \times 10^{-3}$ also explodes when the central temperature is the range dominated by the hot CNO cycle.

As a result of the kinetic energy stored in the rotation of models R1.c and R1.d, the critical metallicity needed to trigger an explosion decreases significantly relative to the non-rotating case. We observe that rotating models with initial metallicities up to $Z_{CNO} = 8 \times 10^{-4}$ do not explode even via the rp-process, which is dominant at temperatures above $T \approx 5 \times 10^8$ K and increases the hydrogen burning rate by $200 - 300$ times relative to the hot CNO cycle. We also note that the evolution time scales of the collapse and bounce phases are reduced because rotating models are more compact and have a higher initial central density and temperature than the spherical ones at the onset of the gravitational instability.

The right panels in Figure 1 show the time evolution of the central rest-mass density (upper panel) and the central temperature (lower panel) for models S2.a, S2.b, R2.a and R2.d, i.e., of models with a mass of $M = 10^6 \mathrm{M}_\odot$. We find that the critical metallicity for an explosion in the spherical case is $Z_{CNO} = 5 \times 10^{-2}$ (model S2.b), while model S2.a with $Z_{CNO} = 3 \times 10^{-2}$ collapses to a BH. We note that the critical metallicity leading to a thermonuclear explosion is higher than the critical value found by Fuller et al. (1986) (i.e., $Z_{CNO} = 1 \times 10^{-2}$) for a spherical SMS with the same mass. The initial metallicity leading to an explosion in the rotating case (model
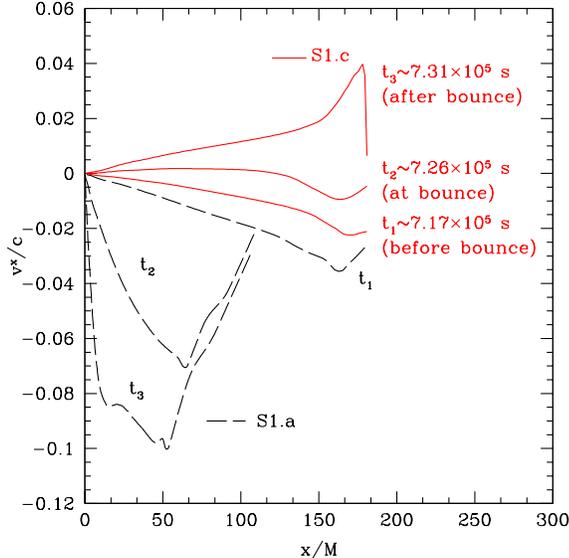
FIG. 2.— Profiles of the x-component of the three-velocity v^x along the x-axis (in the equatorial plane) for the nonrotating spherical stars S1.a (dashed lines) and S1.c (solid lines) at three different time slices near the time at which model S1.c experiences a thermal bounce. Velocity profiles of model S1.c are displayed up to the radius where takes place the formation of a shock that expands into the low density outer layers of the SMS.

R2.d) is more than an order of magnitude smaller than in the spherical case. As for the models with a smaller gravitational mass, the thermal bounce takes place when the physical conditions in the central region of the star allow for the release of energy by hydrogen burning through the hot CNO cycle. Overall, the dynamics of the more massive models indicates that the critical initial metallicity required to produce an explosion increases with the rest-mass of the star.

Figure 3 shows the total nuclear energy generation rate in erg/s for the exploding models as a function of time during the late stages of the collapse just before and after bounce. The main contribution to the nuclear energy generation is due to hydrogen burning by the hot CNO cycle. The peak values of the energy generation rate at bounce lie between several 10^{51}erg/s for the rotating models (R1.d and R2.d), and $\approx 10^{52} - 10^{53}$erg/s for the spherical models (S1.c and S2.b). As expected the maximum nuclear energy generation rate needed to produce an explosion is lower in the rotating models. Moreover, as the explosions are due to the energy release by hydrogen burning via the hot CNO cycle, the ejecta would mostly be composed of ^{4}He.

As a result of the thermal bounce, the kinetic energy rises until most of the energy of the explosion is in the form of kinetic energy. We list in the second but last column of Table 1 the radial kinetic energy after thermal bounce, which ranges between $E_{RK} = 1.0 \times 10^{55}$ergs for the rotating star R1.c, and $E_{RK} = 3.5 \times 10^{57}$ergs for the spherical star S2.b.

6.2. Photon luminosity

Due to the lack of resolution at the surface of the star, it becomes difficult to compute accurately the photosphere and its effective temperature from the criterion that the optical depth is $\tau = 2/3$. Therefore, in order to
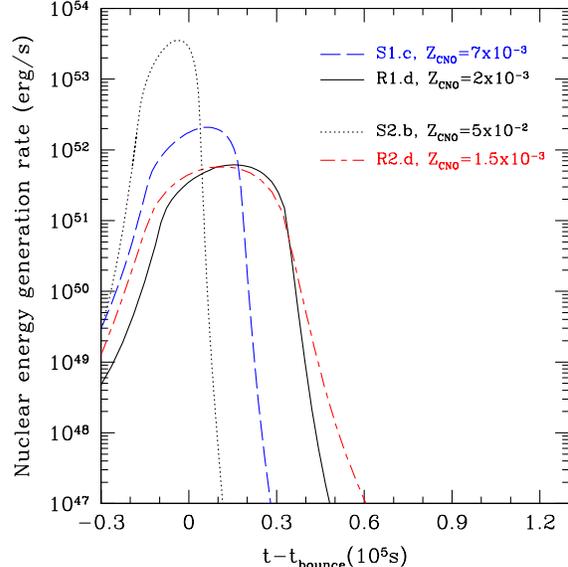

FIG. 3.— Nuclear energy generation rate in erg/s for the exploding models (S1.c, R1.d, R1.c, S2.b and R2.d) as a function of time near the bounce. The contribution to the nuclear energy generation is mainly due to hydrogen burning by the hot CNO cycle. The peak values of the energy generation rate at bounce lie between $\approx 10^{51}$[erg/s] for the rotating models (R1.d and R2.d), and $\approx 10^{52} - 10^{53}$[erg/s] for the spherical models (S1.c and S2.b).

estimate the photon luminosity produced in association with the thermonuclear explosion, we make use of the fact that within the diffusion approximation the radiation flux is given by

$$F_\gamma = -\frac{c}{3\kappa_{es}\rho}\nabla U, \tag{35}$$

where U is the energy density of the radiation, and κ_{es} is the opacity due to electron Thompson scattering, which is the main source of opacity in SMSs. The photon luminosity in terms of the temperature gradient and for the spherically symmetric case can be written as

$$L_\gamma = -\frac{16\pi acr^2 T^3}{3\kappa_{es}\rho}\frac{\partial T}{\partial r}, \tag{36}$$

where a is the radiation constant, and c the speed of light. As can be seen in the last panel of Figure 4 the distribution of matter becomes spherically symmetric during the phase of expansion after the thermonuclear explosion. In this figure (Fig. 4) we show the isodensity contours for the rotating model R1.d. The frames have been taken at the initial time (left figure), at $t = 0.83 \times 10^5$s (central figure) just after the thermal bounce (at $t = 0.78 \times 10^5$s), and at $t = 2.0 \times 10^5$ s when the radius of the expanding matter is roughly 4 times the radius of the star at the onset of the collapse.

The photon luminosity computed using Eq.(36) for model R1.d is displayed in Figure 5, where we also indicate with a dashed vertical line the time at which the thermal bounce takes place. The photon luminosity before the thermal bounce is computed at radii inside the star unaffected by the local dynamics of the low density outer layers which is caused by the initial pressure perturbation and by the interaction between the surface of the SMS and the artificial atmosphere. Once the ex-
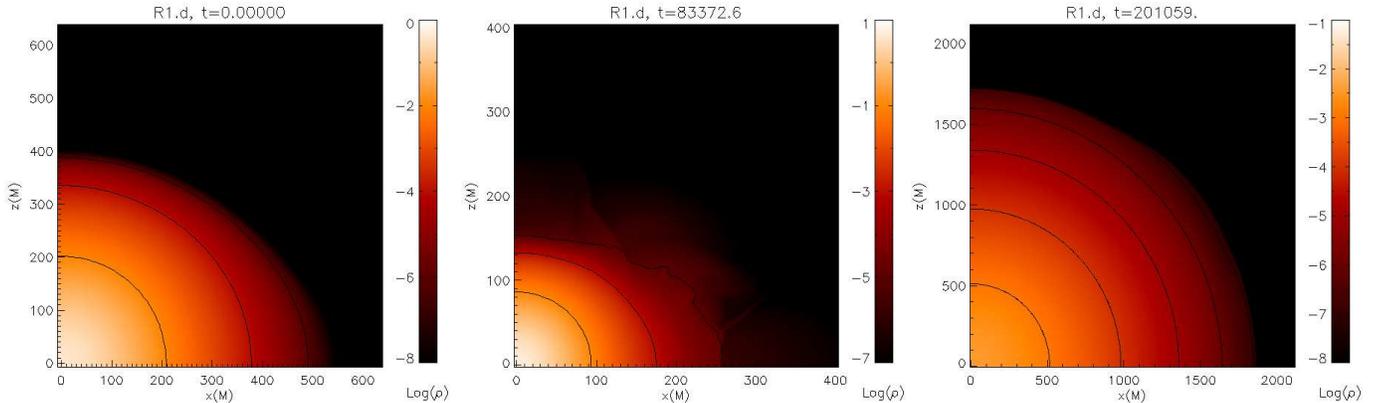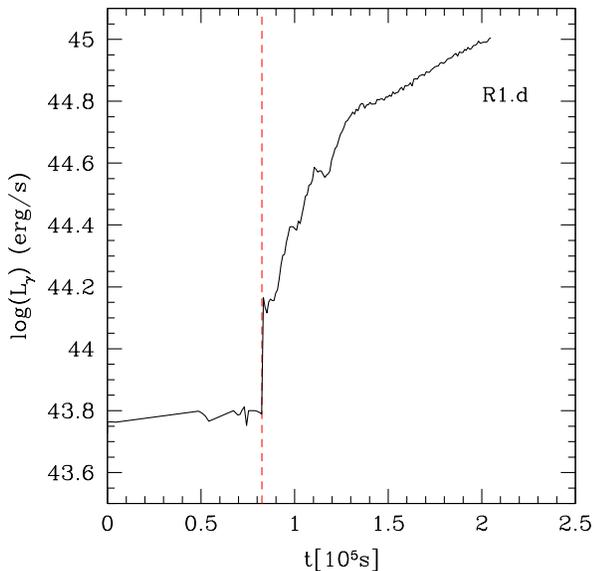
FIG. 4.— Isodensity contours of the logarithm of the rest-mass density (in g/cm^3) for the rotating model R1.d. The frames have been taken at the initial time (left figure), at $t = 0.83 \times 10^5$ s (central figure) just after a thermal bounce takes place, and at $t = 2.0 \times 10^5$ s when the radius of the expanding matter is roughly 4 times the radius of the star at the onset of the collapse.

FIG. 5.— Logarithm of the photon luminosity of model R1.d in units of erg/s as a function of time. The vertical dashed line indicates the time at which the thermal bounce takes place.

panding shock forms near the surface, the photon luminosity is computed near the surface of the star. The lightcurve shows that, during the initial phase, the luminosity is roughly equal to the Eddington luminosity $\approx 5 \times 10^{43}$erg/s until the thermal bounce. Then, the photon luminosity becomes super-Eddington when the expanding shock reaches the outer layers of the star and reaches a value of $L_\gamma \approx 1 \times 10^{45}$erg/s. This value of the photon luminosity after the bounce is within a few percent difference with respect to the photon luminosity Fuller et al. (1986) found for a nonrotating SMS of same rest-mass. The photon luminosity remains super-Eddington during the phase of rapid expansion that follows the thermal bounce. We compute the photon luminosity until the surface of the star reaches the outer boundary of the computational domain $\approx 1.0 \times 10^5$ after the bounce. Beyond that point, the luminosity is expected to decrease, and then rise to a plateau of $\sim 10^{45}$erg/s due to the recombination of hydrogen (see

Fuller et al. 1986 for a nonrotating star).

6.3. Collapse to BH and neutrino emission

The outcome of the evolution of models that do not generate enough nuclear energy during the contraction phase to halt the collapse is the formation of a BH. The evolutionary tracks for the central density and temperature of some of these models are also shown in Figure 1. The central density typically increases up to $\rho_c \sim 10^7$gcm^{-3} and the central temperature up to $T_c \sim 10^{10}$K just before the formation of an apparent horizon.

Three isodensity contours for the rotating model R1.a collapsing to a BH are shown in Figure 6, which display the flattening of the star as the collapse proceeds. The frames have been taken at the initial time (left panel), at $t = 0.83 \times 10^5$s (central panel) approximately when model R1.d with higher metallicity experiences a thermal bounce and, at $t = 1.127 \times 10^5$s, where a BH has already formed and its AH has a mass of 50% of the total initial mass.

At the temperatures reached during the late stages of the gravitational collapse (in fact at $T \geq 5 \times 10^8$K) the most efficient process for hydrogen burning is the break-out from the hot CNO cycle via the $^{15}O(\alpha, \gamma)^{19}$Ne reaction. Nevertheless, we find that models which do not release enough nuclear energy by the hot CNO cycle to halt their collapse to a BH, are not able to produce a thermal explosion due to the energy liberated by the $^{15}O(\alpha, \gamma)^{19}$Ne reaction. We note that above 10^9K, not all the liberated energy is used to increase the temperature and pressure, but is partially used to create the rest-mass of the electron-positron pairs. As a result of pair creation, the adiabatic index of the star decreases, which means the stability of the star is reduced. Moreover, due to the presence of e$^\pm$ pairs, neutrino energy losses grow dramatically.

Figure 7 shows (solid lines) the time evolution of the redshifted neutrino luminosities of four models collapsing to a BH (S1.a, R1.a, S2.a, and R2.a), and (dashed lines) of four models experiencing a thermal bounce (S1.c, R1.d, S2.b, and R2.d). The change of the slope of the neutrino luminosities at $\sim 10^{43}$erg/s denotes the transition from photo-neutrino emission to the pair an-
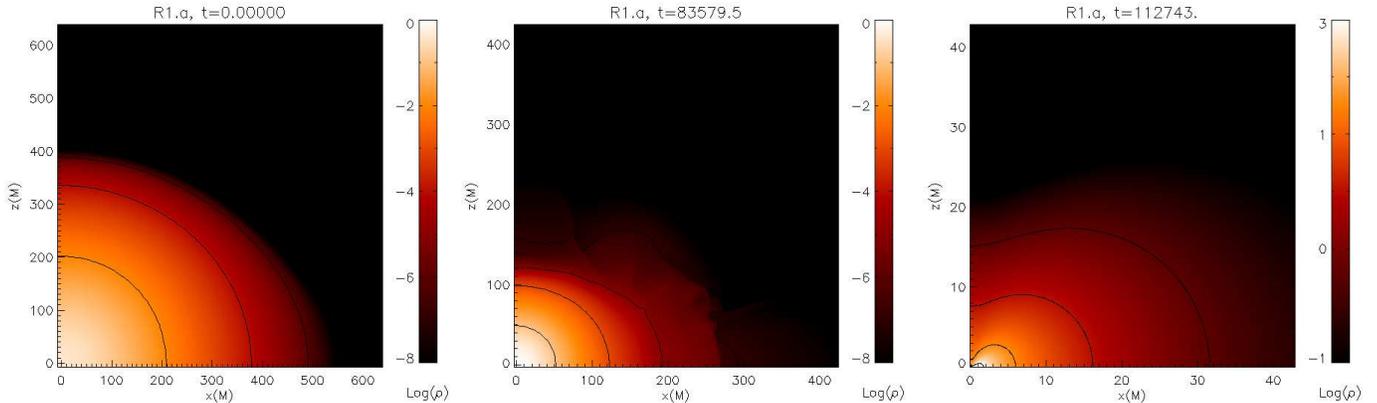
FIG. 6.— Isodensity contours of the logarithm of the rest-mass density (in g/cm^3) for the rotating model R1.a. The frames have been taken at the initial time (left panel), at $t = 0.83 \times 10^5$ s (central panel), at $t = 1.127 \times 10^5$ s, where a BH has already formed and its apparent horizon encloses a mass of 50% of the total initial gravitational mass.

nihilation dominated region. The peak luminosities in all form of neutrino for models collapsing to a BH are $L_\nu \sim 10^{55}$erg/s. Neutrino luminosities can be that important because the densities in the core prior to BH formation are $\rho_c \sim 10^7$gcm^{-3}, and therefore neutrinos can escape. The peak neutrino luminosities lie between the luminosities found by Linke et al. (2001) for the collapse of spherical SMS, and those found by Woosley et al. (1986) (who only took into account the luminosity in the form of electron antineutrino). The maximum luminosity decreases slightly as the rest-mass of the initial model increases, which was already observed by Linke et al. (2001). In addition, we find that the peak of the redshifted neutrino luminosity does not seem to be very sensitive to the initial rotation rate of the star. We also note that the luminosity of model R1.a reflects the effects of hydrogen burning at $L_\nu \sim 10^{43}$erg/s.

The total energy output in the form of neutrinos is listed in the last column of Table 1 for several models. The total radiated energies vary between $E_\nu \sim 10^{56}$ ergs for models collapsing to a BH, and $E_\nu \sim 10^{45} - 10^{46}$ ergs for exploding models. These results are in reasonable agreement with previous calculations. For instance, Woosley et al. (1986) obtained that the total energy output in the form of electron antineutrinos for a spherical SMS with a mass 5×10^5M$_\odot$ and zero initial metallicity was 2.6×10^{56}ergs, although their simulations neglected general relativistic effects which are important to compute accurately the relativistic redshifts. On the other hand, Linke et al. (2001), by means of relativistic one-dimensional simulations, found a total radiated energy in form of neutrinos of about 3×10^{56}ergs for the same initial model, and about 1×10^{56}ergs when redshifts were taken into account. In order to compare with the results of Linke et al. (2001), we computed the redshifted total energy output for Model S1.a, having the same rest-mass, until approximately the same evolution stage as Linke et al. (2001) did (i.e. when the differential neutrino luminosity $dL_\nu/dr \sim 4 \times 10^{45}$erg/s/cm). We find that the total energy released in neutrinos is 1.1×10^{56}ergs.

The neutrino luminosities for models experiencing a thermonuclear explosion (dashed lines in Fig. 7) peak at much lower values $L_\nu \sim 10^{42} - 10^{43}$erg/s, and decrease
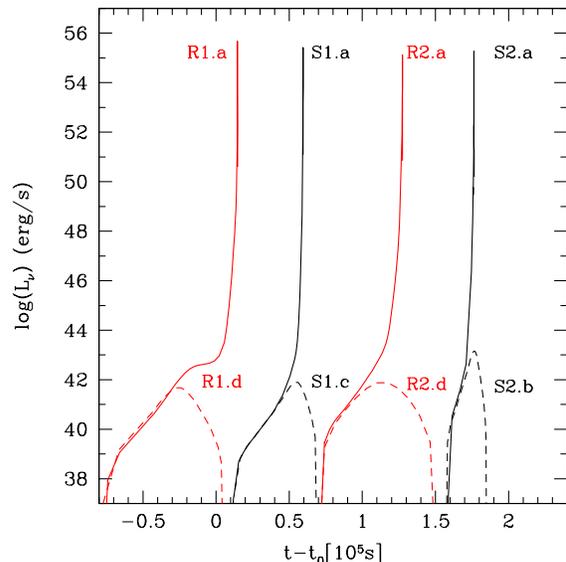

FIG. 7.— Time evolution of the redshifted neutrino luminosities for models R1.a, S1.a, R2.a, and S2.a all collapsing to a BH; and for models R1.d, S1.c, R2.d, and S2.b experiencing a thermal bounce. The time is measured relative to the collapse timescale of each model, R1, S1, R2 and S2, with $t_0 \approx (1, 7, 0.2, 6)$ in units of 10^5s.

due to the expansion and disruption of the star after the bounce.

6.4. Implications for gravitational wave emission

The axisymmetric gravitational collapse of rotating SMSs with uniform rotation is expected to emit a burst of gravitational waves (Saijo et al. 2002; Saijo & Hawke 2009) with a frequency within the LISA low frequency band ($10^{-4} - 10^{-1}$Hz). Although through the simulations presented here we could not investigate the development of nonaxisymmetric features in our axisymmetric models that could also lead to the emission of GWs, Saijo & Hawke (2009) have shown that the three dimensional collapse of rotating stars proceeds in a approximately axisymmetric manner.

In an axisymmetric spacetime, the ×-mode vanishes and the +-mode of gravitational waves with $l = 2$ computed using the quadrupole formula is written as

(Shibata & Sekiguchi 2003)

$$h_+^{quad} = \frac{\ddot{I}_{xx}(t_{ret}) - \ddot{I}_{zz}(t_{ret})}{r} sin^2\theta, \qquad (37)$$

where $\ddot{I}_{ij}$ refers to the second time derivative of the quadrupole moment. The gravitational wave quadrupole amplitude is $A_2(t) = \ddot{I}_{xx}(t_{ret}) - \ddot{I}_{zz}(t_{ret})$. Following Shibata & Sekiguchi (2003) we compute the second time derivative of the quadrupole moment by finite differencing the numerical results for the first time derivative of I_{ij} obtained by

$$\dot{I}_{ij} = \int \rho_* \left(v^i x^j + x^i v^j \right) d^3x. \qquad (38)$$

We calculate the characteristic gravitational wave strain (Flanagan & Hughes 1998) as

$$h_{char}(f) = \sqrt{\frac{2}{\pi}\frac{G}{c^3}\frac{1}{D^2}\frac{dE(f)}{df}}, \qquad (39)$$

where D is the distance of the source, and $dE(f)/df$ the spectral energy density of the gravitational radiation given by

$$\frac{dE(f)}{df} = \frac{c^3}{G}\frac{(2\pi f)^2}{16\pi} \left| \tilde{A}_2(f) \right|^2, \qquad (40)$$

with

$$\tilde{A}_2(f) = \int A_2(t) e^{2\pi i f t} dt. \qquad (41)$$

We have calculated the quadrupole gravitational wave emission for the rotating model R1.a collapsing to a BH. We plot in Figure 8 the characteristic gravitational wave strain (Eq.39) for this model assuming that the source is located at a distance of 50 Gpc (i.e., $z \approx 11$) , together with the design noise spectrum $h(f) = \sqrt{f S_h(f)}$ of the LISA detector (Larson et al. 2000). We find that, in agreement with Saijo et al. (2002), Saijo & Hawke (2009) and Fryer & New (2011), the burst of gravitational waves due to the collapse of a rotating SMS could be detected at a distance of 50 Gpc and at a frequency which approximately takes the form (Saijo et al. 2002)

$$f_{burst} \sim 3 \times 10^{-3} \left(\frac{10^6 M_\odot}{M} \right) \left(\frac{5M}{R} \right)^{3/2} \text{[Hz]}, \qquad (42)$$

where R/M is a characteristic mean radius during black hole formation (typically set to $R/M = 5$).

Furthermore, Kiuchi et al. (2011) have recently investigated, by means of three-dimensional general relativistic numerical simulations of equilibrium tori orbiting BHs, the development of the nonaxisymmetric Papaloizou-Pringle instability in such systems (Papaloizou & Pringle 1984), and have found that a nonaxisymmetric instability associated with the $m = 1$ mode grows for a wide range of self-gravitating tori orbiting BHs, leading to the emission of quasiperiodic GWs. In particular, Kiuchi et al. (2011) have pointed out that the emission of quasiperiodic GWs from the torus resulting after the formation of a SMBH via the collapse of a SMS could be well above the noise sensitivity curve of LISA for sources located at a distance of 10Gpc. The
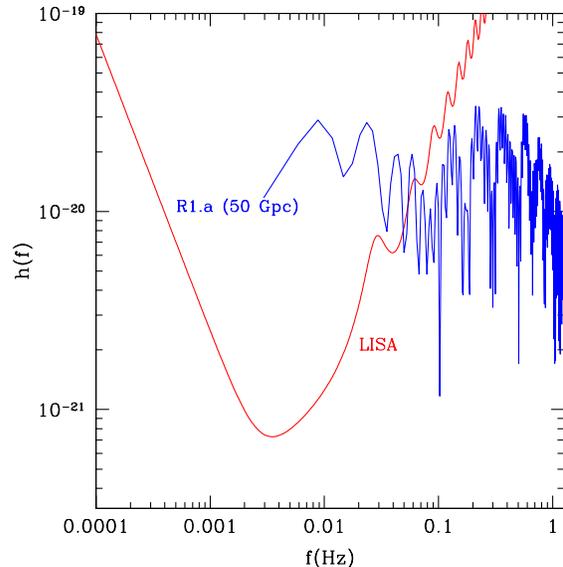

FIG. 8.— Characteristic gravitational wave strain for model R1.a assuming that the source is located at a distance of 50 Gpc, together with the design noise spectrum $h(f) = \sqrt{f S_h(f)}$ for LISA detector.

development of the nonaxisymmetric Papaloizou-Pringle instability during the evolution of such tori would lead to the emission of quasiperiodic GWs with peak amplitude $\sim 10^{-18}-10^{-19}$ and frequency $\sim 10^{-3}$Hz and maintained during the accretion timescale $\sim 10^5$s.

6.5. Conclusions

We have presented results of general relativistic simulations of collapsing supermassive stars using the two-dimensional general relativistic numerical code Nada, which solves the Einstein equations written in the BSSN formalism and the general relativistic hydrodynamic equations with high resolution shock capturing schemes. These numerical simulations have used an EOS that includes the effects of gas pressure, and tabulated those associated with radiation pressure and electron-positron pairs. We have also taken into account the effects of thermonuclear energy release by hydrogen and helium burning. In particular, we have investigated the effects of hydrogen burning by the β-limited hot CNO cycle and its breakout via the $^{15}O(\alpha,\gamma)^{19}$Ne reaction (rp-process) on the gravitational collapse of nonrotating and rotating SMSs with non-zero metallicity.

We have found that objects with a mass of $\approx 5 \times 10^5$M$_\odot$ and an initial metallicity greater than $Z_{CNO} \approx 0.007$ explode if non-rotating, while the threshold metallicity for an explosion is reduced to $Z_{CNO} \approx 0.001$ for objects which are uniformly rotating. The critical initial metallicity for a thermal explosion increases for stars with a mass of $\approx 10^6$M$_\odot$. The most important contribution to the nuclear energy generation is due to the hot CNO cycle. The peak values of the nuclear energy generation rate at bounce range from $\sim 10^{51}$erg/s for rotating models (R1.d and R2.d), to $\sim 10^{52} - 10^{53}$erg/s for spherical models (S1.c and S2.b). After the thermal bounce, the radial kinetic energy of the explosion rises until most of the energy is kinetic, with values ranging from $E_K \sim 10^{56}$ergs for rotating stars, to up

$E_K \sim 10^{57}$ergs for the spherical star S2.b. The neutrino luminosities for models experiencing a thermal bounce peak at $L_\nu \sim 10^{42}$erg/s.

The photon luminosity roughly equal to the Eddington luminosity during the initial phase of contraction. Then, after the thermal bounce, the photon luminosity becomes super-Eddington with a value of about $L_\gamma \approx 1 \times 10^{45}$erg/s during the phase of rapid expansion that follows the thermal bounce. For those stars that do not explode we have followed the evolution beyond the phase of black hole formation and computed the neutrino energy loss. The peak neutrino luminosities are $L_\nu \sim 10^{55}$erg/s.

SMSs with masses less than $\approx 10^6 M_\odot$ could have formed in massive halos with $T_{vir} \gtrsim 10^4$K. Although the amount of metals that was present in such environments at the time when SMS might have formed is unclear, it seems possible that the metallicities could have been smaller than the critical metallicities required to reverse the gravitational collapse of a SMS into an explosion. If so, the final fate of the gravitational collapse of rotating SMSs would be the formation of a SMBH and a torus. In a follow-up paper, we aim to investigate in detail the dynamics of such systems (collapsing of SMS to a BH-torus system) in 3D, focusing on the post-BH evolution and the development of nonaxisymmetric features that could emit detectable gravitational radiation.

REFERENCES

Alcubierre M., Brandt S., Brügmann B., Holz D., Seidel E., Takahashi R. & Thornburg J. 2001, Int. J. Mod. Phys. D10

Alcubierre M., Brügmann B., Diener P., Koppitz M., Pollney D., Seidel E. & Takahashi R. 2003, Phys. Rev. D, 67, 084023

Alvarez M. A., Wise J. H. & Abel T. 2009, ApJ, 701, L133

Appenzeller & Fricke 1972

Baumgarte T. W. & Shapiro S. L. 1999, ApJ, 526, 937

Baumgarte T. W. & Shapiro S. L. 1999, ApJ, 526, 941

Baumgarte T. W. & Shapiro S. L. 1999, Phys. Rev. D, 59, 024007

Begelman M. C. 2009, MNRAS, 402, 673

Begelman M. C. & Shlosman I. 2009, ApJ, 702, L5

Begelman M. C., Volonteri M. & Rees M. J. 2006, MNRAS, 370, 289

Bona C., Massó J., Seidel E. and Stela J. 1997, Phys. Rev. D, 56, 3405

Bromm V. & Loeb A. 2003, ApJ, 596, 34

Campanelli M., Lousto C. O., Marronetti P. & Zlochower Y. 2006, Phys. Rev. D, 96, 111101

Chandrasekhar S. 1964, ApJ, 140

Clayton D.D. 1983, in Principles of Stellar Evolution and Nucleosynthesis, Univ. Chicago Press, 366

Einfeldt B. 1988, SIAM J. Numer. Anal., 25, 294

Fan, X. 2006, New Astronomy Reviews, 50, 665

Flanagan, E. E. & Hughes S.A 1998, prd, 57, 4535

Freese K., Ilie C., Spolyar D., Valluri M. & Bodenheimer P. 2010, ApJ, 716, 1397

Fryer C. L. & New K. C. B. 2011, Living Reviews in Relativity, 14, 1

Fowler W. S. 1964, Rev.Mod.Phys., 36, 545

Fowler W. S. & Hoyle F. 1964, Rev.Mod.Phys., 36, 545

Fuller G. M., Woosley S. E. & Weaver T.A. 1986, ApJ307, 675

Genzel R., Picho C., Eckart A., Gerhard O.E. & Ott T. 2000, MNRAS, 317, 348

Haft M., Raffelt G. & Weiss A. 1994, ApJ, 425, 222

Haiman Z. & Loeb A. 2001, ApJ, 552, 459

Harten A., Lax P. D., & van Leer B. 1983, SIAM Rev., 25, 35

Hawke I., Löffler F. & Nerozzi A. 2005, Phys. Rev. D, 71, 104006

Hoyle F. & Fowler W. A. 1963, MNRAS, 125, 169

Iben I. 1963, ApJ, 138, 1090

Itoh N., Hayashi H., Nishikawa A. & Kohyama Y. 1996, ApJS, 102, 441

Kormendy J. & Gebhardt K. 2001, AIP Conference Proceedings: 20th Texas Symposium, 586, 363

Kiuchi K., Shibata M., Montero P. J. & Font J. A. 2011, Phys. Rev. Lett., 106, 251102

Larson S. L., Hiscock W. A. & Hellings R. W. 2000, Phys. Rev. D, 62, 062001

Linke F., Font J. A., Janka H.-T., Müller E. & Papadopoulos P. 2001, A&A, 376, 568

Montero P. J., Font J. A. & Shibata M. 2008, Phys. Rev. D, 78, 064037

Nakamura T., Oohara K. & Kojima Y. 1987, Prog. Theor. Phys. Suppl., 90, 1

New K. C. B. & Shapiro S. L. 2001, ApJ, 548, 439

Omukai K., Schneider R. & Haiman Z. 2008, ApJ, 686, 801

Papaloizou J. C. B. & Pringle J. E. 1984, MNRAS, 208, 721

Rees M. J. 1998, in Black Holes and Relativistic Stars, ed. R. M. Wald, Univ. Chicago Press, 79

Rees M. J. 2001, in Black Holes in Binaries and Galactic Nuclei, ed. L. Kaper, E. P. J. van de Heurel, and P.A. Woudt, New York Springer, 351

Saijo M., Baumgarte T.H., Shapiro S.L. & Shibata M. 2002, ApJ, 569, 349

Saijo M. & Hawke I. 2009, Phys. Rev. D, 80, 064001

Santoro F. & Shull M. J. 2006, ApJ, 643, 26

Shapiro S. L. & Teukolsky S. A. 1979, ApJ, 234, L177

Shibata M., Phys. Rev. D, 55, 2002

Shibata M. 2003, Phys. Rev. D, 67, 024033

Shibata M. & Sekiguchi Y. I. 2003, Phys. Rev. D, 68, 104020

Shibata M. & Shapiro S. L. 2002, ApJ, 572, L39

Shibata M. & Nakamura T. 1995, Phys. Rev. D, 52, 5428

Shen K. & Bildsten L. 2007, ApJ, 660, 1444

Shlosman I., Frank J. & Begelman M. C. 1989, Nature, 338, 45

Spiteri R. J. & Ruuth S. J. 2002, SIAM J. Num. Analysis, 40, 2, 469

Spolyar D., Freese K. & Gondolo P. 2008, Phys. Rev. Lett., 100, 051101

Thornburg J. 2007, Living Rev. Relativity 10, 743

Volonteri M. 2010, A&ARv, 18, 279

Yoo J. & Miralda-Escudé J. 2004, ApJ, 614, L25

Wiescher M., Görres J. & Schatz H., J. Phys. G 1999, 25, R133

Woosley S. E., Wilson J. R. & Mayle R. 1986, ApJ302, 19